

KEK Preprint 2001-20

Belle Preprint 2001-6

Study of Rare B Meson Decays at Belle

Toru Iijima

*High Energy Accelerator Research Organization (KEK), 1-1 Oho, Tsukuba, Japan**E-mail: toru.iijima@kek.jp*

for the Belle Collaboration

Abstract

In this paper, we briefly review results on rare decays of B mesons from the Belle experiment, based on 10.4 fb^{-1} data collected on the $\Upsilon(4S)$ resonance. The topics include measurements of Cabibbo suppressed decays $B \rightarrow D^{(*)}K^{(*)}$, charmless two-body decays $B \rightarrow \pi\pi$, $K\pi$, KK and $B \rightarrow \eta' h$ ($h = K^+, \pi^+, K^0$), and a search for flavor changing neutral current decays $B \rightarrow K^{(*)}\ell^+\ell^-$.

*To appear in the Proceedings of the**4th International Workshop on B Physics and CP Violation (BCP4)**February 19–23, 2001, Ise-Shima, Japan.*

1 Introduction

Rare decays of the B meson proceed via a variety of diagrams. They provide a unique opportunity to study the Kobayashi-Maskawa matrix elements, $|V_{cb}|$, $|V_{ub}|$, $|V_{ts}|$ and $|V_{td}|$, as well as their relative phases. In addition, decays involving loop diagrams are interesting because of their sensitivity to effects of new physics. Such rare B meson decays can be studied in detail at the recently commissioned e^+e^- B -factories, KEKB and PEP-II.

By the end of December 2000, the Belle experiment [1] at the KEKB accelerator [2] had accumulated 10.4fb^{-1} of data on the $\Upsilon(4S)$ resonance, corresponding to 11.1×10^6 $B\bar{B}$ pairs. Based on this data set, results for the following rare decays are briefly reviewed in this paper; 1) Cabibbo suppressed decays $B \rightarrow D^{(*)}K^{(*)}$, 2) charmless two-body decays $B \rightarrow \pi\pi$, $K\pi$, KK , 3) charmless decays involving the η' meson $B \rightarrow \eta' h$ ($h = K^+, \pi^+, K^0$), and 4) a search for flavor changing neutral current (FCNC) decays $B \rightarrow K^{(*)}\ell^+\ell^-$. Results for additional rare decay modes can be found in other contributions to this conference [3].

In all the analyses, B candidates are reconstructed using the beam constrained mass, $m_{bc} = \sqrt{E_{\text{beam}}^2 - p_B^2}$, and the energy difference, $\Delta E = E_B - E_{\text{beam}}$. Here, $E_{\text{beam}} \equiv \sqrt{s}/2 \simeq 5.290$ GeV, and p_B and E_B are the momentum and energy of the reconstructed B in the $\Upsilon(4S)$ rest frame, respectively ^a. Normally we compute ΔE assuming a π mass for each charged particle from B decays. This shifts ΔE by about -50 MeV for each K^\pm meson. Other common analysis techniques, the particle identification (PID) cut and the $q\bar{q}$ background suppression cut, are described in appendices. Throughout this paper, the inclusion of charge conjugate states is implied, except for the direct CP

^aIn the analysis for the Cabibbo suppressed decays, described in Sec. 2, the beam constrained mass is calculated in the laboratory frame as $m_{bc} = \sqrt{(E_B^{lab})^2 - |\vec{p}_B^{lab}|^2}$. Here \vec{p}_B^{lab} is the B candidate's laboratory momentum vector and $E_B^{lab} = \frac{1}{E_{ee}}(s/2 + \vec{P}_{ee} \cdot \vec{p}_B^{lab})$, where s is square of the center of mass energy, and \vec{P}_{ee} and E_{ee} are the laboratory momentum and energy of the e^+e^- system, respectively.

violation measurement described in Sec. 3. The first and second errors in results represent statistical and systematic errors, respectively.

2 Cabibbo Suppressed Decays

Direct CP -violating asymmetries due to interference between $b \rightarrow c$ and $b \rightarrow u$ transition amplitudes in the Cabibbo suppressed $B^- \rightarrow D^0 K^-$ decay is a theoretically clean way to determine the ϕ_3 angle of the unitarity triangle [4]. As a first step of this program, we have searched for the Cabibbo suppressed processes $B^- \rightarrow D^{*0} K^-$, $\bar{B}^0 \rightarrow D^{*+} K^-$, $\bar{B}^0 \rightarrow D^+ K^-$ as well as $B^- \rightarrow D^0 K^-$. In the tree level approximation, their branching fractions are related to those of the Cabibbo favored $B \rightarrow D^{(*)} \pi^-$ counterparts by

$$R \equiv \frac{\mathcal{B}(B \rightarrow D^{(*)} K^-)}{\mathcal{B}(B \rightarrow D^{(*)} \pi^-)} \simeq \tan^2 \theta_C (f_K/f_\pi)^2 \simeq 0.074, \quad (1)$$

using the Cabibbo angle θ_C and the meson decay constants $f_{K(\pi)}$ ^b. The only Cabibbo suppressed decay observed to date is $B^- \rightarrow D^0 K^-$, reported by CLEO [5] with $R = 0.055 \pm 0.014 \pm 0.005$.

In the analysis, D mesons are reconstructed using the decay modes, $D^0 \rightarrow K^- \pi^+$, $K^- \pi^+ \pi^0$, $K^- \pi^+ \pi^+ \pi^-$ and $D^+ \rightarrow K^- \pi^+ \pi^+$, $K_S^0 \pi^+$, $K_S^0 \pi^+ \pi^+ \pi^-$, $K^- K^+ \pi^+$. For D^{*0} and D^{*+} reconstruction, $D^{*0} \rightarrow D^0 \pi^0$ and $D^{*+} \rightarrow D^0 \pi^+$, $D^+ \pi^0$ decays are used. If multiple entries are found in one event, the best candidate is selected based on a χ^2 determined from the differences between measured and nominal masses of m_D , m_{bc} and, when appropriate $m_{D^*} - m_D$ and m_{π^0} (π^0 from the D^* decays). To suppress the much more abundant $B \rightarrow D^{(*)} \pi^-$ decays, a relatively tight PID cut $\mathcal{R}_K > 0.8$, which gives 76.5% efficiency for K tracks and 2% $\pi \rightarrow K$ fake rate, is applied for the prompt hadron track from the B decay (see Appendix A).

^b The relation assumes the validity of factorization and flavor- $SU(3)$ symmetry.

Figure 1 shows the ΔE distributions for all $B \rightarrow D^{(*)}\pi^-$ ($\mathcal{R}_K < 0.8$) and $B \rightarrow D^{(*)}K^-$ ($\mathcal{R}_K > 0.8$) enriched samples. In all the $B \rightarrow D^{(*)}K$ channels, signal peaks are clearly seen at $\Delta E = -49$ MeV. Table 1 summarizes the results. The R ratios, defined in Eq.(1), are calculated from the extracted yields of $B \rightarrow D^{(*)}\pi^-$ and $B \rightarrow D^{(*)}K^-$ decays by taking into account the difference in the reconstruction efficiencies. In all cases, the R ratios are consistent within errors with the expectation in Eq.(1). These are the first observations of the $B \rightarrow D^+K^-$, $D^{*0}K^-$ and $D^{*+}K^-$ decay processes ^c.

We have also searched for the $B^- \rightarrow D^0K^{*-}$ decay mode. The K^* mesons are reconstructed using the clean $K_S^0\pi^-$ channel. The first observed evidence of this decay mode is shown in Fig. 2. The signal yield is 15.0 ± 4.6 with a statistical significance of 4.6σ . The branching fraction normalized to that of $B^- \rightarrow D^0\pi^-$ is found to be $0.116 \pm 0.036 \pm 0.015$ (preliminary) ^d.

3 $B \rightarrow \pi\pi, K\pi, KK$ Decays

Branching fraction measurements of the $B \rightarrow \pi\pi, K\pi$ and KK decays are an important first step toward indirect and direct CP violation studies with the $\pi\pi$ and $K\pi$ modes, which are related to the angles ϕ_2 and ϕ_3 of the unitarity triangle, respectively. Moreover, assuming isospin and $SU(3)$ symmetry, recent theoretical work suggests that branching fraction of these modes can be used to extract or place limits on the angles ϕ_2 and ϕ_3 [6].

We have analyzed the data for the $B^0 \rightarrow \pi^+\pi^-, K^+\pi^-, K^+K^-, K^0\pi^0$ and $B^+ \rightarrow \pi^+\pi^0, K^+\pi^0, K^0\pi^+$ decays. The Belle detector is equipped with a high momentum PID system, which gives clear separation between the charged π and K mesons in these final states. The π and K mesons are distinguished by the PID cut $\mathcal{R}_{\pi(K)} > 0.6$, which gives 92.4%

^c Results on $B \rightarrow D^{(*)}K$ modes were updated after the conference.

^d The ratio similar to Eq.(1), $R \equiv \mathcal{B}(B^- \rightarrow D^0K^{*-})/\mathcal{B}(B^- \rightarrow D^0\rho^-)$, is not presented here because our analysis for the Cabibbo favored counterpart $B^- \rightarrow D^0\rho^-$ has not been completed yet.

efficiency and 4.3% fake rate (true π fakes K) for π mesons and 84.9% efficiency and 10.4% fake rate (true K fakes π) for K mesons, respectively (see Appendix A). The dominant background from the continuum $q\bar{q}$ process is suppressed using the likelihood ratio method described in Appendix B.

Figure 3 shows m_{bc} and ΔE distributions for the $\pi^+\pi^-$, $K^+\pi^-$ and $K_S^0\pi^+$ modes. Each distribution is fitted to a Gaussian signal on top of a background function, which is modeled by the ARGUS background function [7] for m_{bc} and by a linear function for ΔE . The ΔE fit results are used to determine the signal yields. For the $\pi^+\pi^-$ and $K^+\pi^-$ modes, the cross-talk from each mode is not negligible, and thus the fits treat the size of both components as free parameters. The cross talk found in these fits are consistent with expectations. Figure 4 shows the m_{bc} and ΔE projections for the $\pi^+\pi^0$, $K^+\pi^0$ and $K_S^0\pi^0$ modes. For these modes, since the ΔE distribution has a long tail, a two-dimensional fit is applied to the m_{bc} and ΔE distributions. For the $\pi^+\pi^0$ mode, since the cross talk from $K^+\pi^0$ is significant and separated by less than 1σ in ΔE , the fit includes the expected $K^+\pi^0$ component.

Results of the branching fraction measurements are summarized in Table 2 ^e. The charge averaged branching fractions for $B \rightarrow \pi^+\pi^-$, $K^+\pi^-$, $K^+\pi^0$, $K^0\pi^+$, and $K^0\pi^0$ are measured with statistically significant signals. Our results are consistent with other measurements [8]:[9], confirm that $\mathcal{B}(B^0 \rightarrow K^+\pi^-)$ is larger than $\mathcal{B}(B^0 \rightarrow \pi^+\pi^-)$, and indicate that $\mathcal{B}(B^+ \rightarrow h^+\pi^0)$ and $\mathcal{B}(B^0 \rightarrow K^0\pi^0)$ is larger than expected in relation to the $B^0 \rightarrow h^+\pi^-$ and $B^+ \rightarrow K^0\pi^+$ modes based on isospin or penguin dominance [6].

We have also searched for direct CP violation in $B \rightarrow K^\pm\pi^\mp$ and $B \rightarrow K^\pm\pi^0$ modes. With the high momentum PID at Belle, the dilution of the CP asymmetry due to double misidentification is as small as $\sim 0.5\%$. Inherent asymmetries in the Belle detector are determined to be less than 2% based on the yield difference between $\bar{D}^0 \rightarrow K^+\pi^-$ and

^e Results shown in Table 2 were updated after the conference.

$D^0 \rightarrow K^- \pi^+$ decays. Figure 5-a) and b) shows the ΔE distributions for the $K^- \pi^+$ and $K^+ \pi^-$ final states. The signal yields, extracted with the same procedure as the branching fraction measurement, are $27.7^{+6.8}_{-6.1}$ for $B^0 \rightarrow K^- \pi^+$ and $25.4^{+7.0}_{-6.3}$ for $\bar{B}^0 \rightarrow K^+ \pi^-$, giving a partial rate asymmetry $^f \mathcal{A}_{cp}(K^\pm \pi^\mp) = 0.043 \pm 0.175 \pm 0.021$ and its 90% confidence level interval $-0.26 < \mathcal{A}_{cp}(K^\pm \pi^\mp) < 0.35$. Figure 5-c) and d) show the same distributions for the $K^- \pi^0$ and $K^+ \pi^0$ final states. The yields are $18.3^{+5.6}_{-4.9}$ for $B^- \rightarrow K^- \pi^0$ and $17.6^{+5.5}_{-4.8}$ for $B^+ \rightarrow K^+ \pi^0$, giving $\mathcal{A}_{cp}(K^\pm \pi^0) = 0.019^{+0.219}_{-0.191}$ (only statistical error is shown for this mode). It should be noted that these results on A_{cp} are preliminary.

4 $B \rightarrow \eta' h$ Decays

Measurements by CLEO [10] and BABAR [9] indicate that the branching fraction for $B \rightarrow \eta' K$ is significantly larger than theoretical expectations. Here, we present preliminary results for the $B^+ \rightarrow \eta' K^+$, $\eta' \pi^+$ and $B^0 \rightarrow \eta' K^0$ decay modes. The η' mesons are reconstructed using $\eta' \rightarrow \eta \pi \pi$, $\eta \rightarrow \gamma \gamma$ and $\eta' \rightarrow \rho \gamma$ decays. The $q\bar{q}$ background is suppressed by a likelihood ratio cut similar to that used for the $B \rightarrow \pi \pi$, $K \pi$, KK analysis. The likelihood contains SFW and $\cos \theta_B$ (see Appendix B). The prompt charged K/π from the B decay is separated by the PID cut $\mathcal{R}_{\pi(K)} > 0.6$.

Figure 6 shows the m_{bc} and ΔE distributions for the signal candidates. By combining results for the two sub-decay modes of the η' meson, the observed signals have statistical significances of 10.9σ and 5.9σ for the $\eta' K^+$ and $\eta' K^0$ modes, respectively. Their branching fractions are found to be $\mathcal{B}(B^+ \rightarrow \eta' K^+) = (6.8^{+1.3}_{-1.2} \ ^{+0.7}_{-0.9}) \times 10^{-5}$ and $\mathcal{B}(B^0 \rightarrow \eta' K^0) = (6.4^{+2.5}_{-2.0} \ ^{+1.0}_{-1.1}) \times 10^{-5}$. In the $\eta' \pi^+$ mode, no statistically significant signal is seen, and we set an upper limit of $\mathcal{B}(B^+ \rightarrow \eta' \pi^+) < 1.2 \times 10^{-5}$ (90% C.L.). These results are consistent with the previous measurements.

^f Here the partial rate asymmetry \mathcal{A}_{cp} is defined as, $\mathcal{A}_{cp} \equiv \frac{N(\bar{B} \rightarrow \bar{f}) - N(B \rightarrow f)}{N(\bar{B} \rightarrow \bar{f}) + N(B \rightarrow f)}$.

5 Search for $B \rightarrow K^{(*)}\ell^+\ell^-$ Decays

The FCNC decay, $B \rightarrow K^{(*)}\ell^+\ell^-$, proceeds via loop diagrams, and therefore is sensitive to new physics such as charged Higgs and SUSY. We have searched for the FCNC decays, $B^0 \rightarrow K^{*0}\ell^+\ell^-$, $B^+ \rightarrow K^{*+}\ell^+\ell^-$, $B^0 \rightarrow K^0\ell^+\ell^-$, $B^+ \rightarrow K^+\ell^+\ell^-$, in both electron and muon channels.

The K^0 mesons are reconstructed using $K_S^0 \rightarrow \pi^+\pi^-$ decays. The K^* mesons are reconstructed using $K^{*0} \rightarrow K^+\pi^-$, $K_S^0\pi^0$ and $K^{*+} \rightarrow K_S^0\pi^+$, $K^+\pi^0$ decays. Electrons with $p_{tab} > 0.5 \text{ GeV}/c$ and muons with $p_{tab} > 1.0 \text{ GeV}/c$ are selected with pion fake rates expected at a level of 0.3% and 1.7%, respectively.

Background from $q\bar{q}$ processes is suppressed by a likelihood ratio cut (see Appendix B), where the likelihood contains $\cos\theta_B$, $\cos\theta_{da}$ and a Fisher discriminant constructed from virtual calorimeter variables[11] and the normalized second order Fox-Wolfram momentum R_2 . The largest source of $B\bar{B}$ background are events where both B mesons decay into $\ell\nu X$. This source is suppressed by cutting on a likelihood ratio based on visible energy and $\cos\theta_B$. The large background from $J/\psi \rightarrow \ell^+\ell^-$ and $\psi' \rightarrow \ell^+\ell^-$ decays is vetoed by applying the di-lepton mass cuts, $-0.15 < M_{ee} - M_{J/\psi(\psi')} < 0.07 \text{ GeV}/c^2$ and $-0.10 < M_{\mu\mu} - M_{J/\psi(\psi')} < 0.05 \text{ GeV}/c^2$. The di-electron mass is required to be larger than $0.1 \text{ GeV}/c^2$ to avoid background from π^0 Dalitz decays and γ conversions.

No statistically significant signals have been observed yet, and upper limits at 90% confidence level are set for each mode, which are shown in Fig. 7 along with a comparison to theoretical expectations [12] and the results from previous experiments [13][14][15]. Our upper limits are more restrictive than those of previous experiments, except for the $K^{*0}\mu\mu$ channel.

6 Summary

In this paper, we briefly review results for some B meson rare decays from the Belle experiment, based on 10.4 fb^{-1} data collected on the $\Upsilon(4S)$ resonance. They are summarized as follows,

- Cabibbo suppressed decays $B \rightarrow D^{(*)}K$ have been observed with nearly the expected size relative to $B \rightarrow D^{(*)}\pi$ decays. We claim the first observation of the four modes, $B \rightarrow D^+K^-$, $D^{*0}K^-$, $D^{*+}K^-$ and D^0K^{*-} .
- Our results for the $B \rightarrow \pi\pi$, $K\pi$, KK modes are consistent with other measurements, confirm the small $\pi\pi/K\pi$ ratio, and indicate that the $K^0\pi^0$ mode is larger than theoretically expected.
- The large branching fractions for the $B \rightarrow \eta'K^+$ and $\eta'K^0$ modes are also confirmed.
- Improved upper limits on the FCNC decays $B \rightarrow K^{(*)}\ell^+\ell^-$ are obtained except for the $K^{*0}\mu^+\mu^-$ channel.

In the near future, we anticipate results on various rare B meson decays with much higher statistics and better sensitivity than ever before achieved.

Acknowledgments

We wish to thank the KEKB accelerator group for the excellent operation of the KEKB accelerator. We acknowledge support from the Ministry of Education, Culture, Sports, Science, and Technology of Japan and the Japan Society for the Promotion of Science; the Australian Research Council and the Australian Department of Industry, Science and Resources; the Department of Science and Technology of India; the BK21 program of the Ministry of Education of Korea and the CHEP SRC program of the Korea Science

and Engineering Foundation; the Polish State Committee for Scientific Research under contract No.2P03B 17017; the Ministry of Science and Technology of Russian Federation; the National Science Council and the Ministry of Education of Taiwan; the Japan-Taiwan Cooperative Program of the Interchange Association; and the U.S. Department of Energy.

Appendix A: particle identification cut

A clear separation of charged π and K mesons is essential to find some rare decay signals. We combine outputs from three sub-detectors, specific ionization loss in the central drift chamber (dE/dx), time-of-flight measured by scintillation counter arrays (TOF) and light yields measured by the aerogel Cherenkov counter arrays (ACC), into a likelihood for each particle assumption $\mathcal{L}_{K(\pi)} \equiv \mathcal{L}_{K(\pi)}^{dE/dx} \times \mathcal{L}_{K(\pi)}^{TOF} \times \mathcal{L}_{K(\pi)}^{ACC}$. The particle identification is then performed by cutting on the likelihood ratio $\mathcal{R}_{K(\pi)} \equiv \mathcal{L}_{K(\pi)}/(\mathcal{L}_K + \mathcal{L}_\pi)$. For prompt π and K mesons from B decays, TOF does not provide useful separation, and only dE/dx and ACC information are used. The PID cut efficiency and fake rate are measured using kinematically selected $D^{*+} \rightarrow D^0\pi^+$, $D^0 \rightarrow K^-\pi^+$ decays.

Appendix B: continuum suppression cut

To distinguish $B\bar{B}$ events from the $q\bar{q}$ background, Belle has developed a new event shape variable called ‘‘Super Fox-Wolfram’’. The usual Fox-Wolfram moments are defined as $H_l = \sum_{i,j} |\vec{p}_i| |\vec{p}_j| P_l(\cos\theta_{ij})$, where the indices i and j run over all final state particles, \vec{p}_i and \vec{p}_j are the momentum vectors of the particle i and j , P_l is the l -th Legendre polynomial, and θ_{ij} is the angle between the two particles. In the new method, the normalized Fox-Wolfram moments, $R_l = H_l/H_0$, are decomposed into three terms: $R_l = R_l^{ss} + R_l^{so} + R_l^{oo} = (H_l^{ss} + H_l^{so} + H_l^{oo})/H_0$, where the indices ss , so , and oo indicate

respectively that both, one, or neither of the particles comes from a B candidate. These are combined into a six term Fisher discriminant (Super Fox-Wolfram), defined as $SFW = \sum_{l=1}^4 (\alpha_l R_l^{so} + \beta_l R_l^{oo})$, where α_l and β_l are Fisher coefficients and $l=2,4$ for α_l and R_l^{so} . The terms R_l^{ss} and $R_{l=1,3}^{so}$ are excluded because they are strongly correlated with m_{bc} and ΔE .

We then combine different $q\bar{q}$ suppression variables into a single likelihood, $\mathcal{L}_{s(q\bar{q})} = \prod_i \mathcal{L}_{s(q\bar{q})}^i$, where the $\mathcal{L}_{s(q\bar{q})}^i$ denotes the signal ($q\bar{q}$) likelihood of the suppression variable i , and select candidate events by cutting on the likelihood ratio $\mathcal{R}_s = \mathcal{L}_s / (\mathcal{L}_s + \mathcal{L}_{q\bar{q}})$. The variables used depend on the decay mode. For example, Fig. 8 illustrates the separation of the signal and the $q\bar{q}$ background in the case of $B \rightarrow \pi^+\pi^-, K^+\pi^-, K^+K^-$ analysis, described in Sec. 3, where the likelihood contains the above SFW , the B candidate flight direction ($\cos\theta_B$), and the decay axis direction ($\cos\theta_{da}$). By requiring $\mathcal{R}_s > 0.8$, 97% of the $q\bar{q}$ background is removed while 48% of the signal are kept. In the case of $B \rightarrow \pi^+\pi^0, K^+\pi^0, K^0\pi^0$ modes, the event sphericity (S) and the angle between the thrust axis of the B candidate and that of all the remaining particles (θ_T) are also used. In these modes, since the continuum background is more severe, a loose cut on $\cos\theta_T$ is applied first. Then SFW is extended to include $\cos\theta_T$ and S , and this extended SFW and $\cos\theta_B$ are combined into the likelihood.

References

- [1] Belle Collaboration, K. Abe *et al.*, KEK Progress Report 2000-4 (2000), to be published in Nucl. Inst. and Meth. A.
- [2] KEKB B Factory Design Report, KEK Report 95-7 (1995), unpublished.
- [3] Belle Collaboration, A.Bozek, contribution to these proceedings; A.Garmash, *ibid.*; Y.Ushiroda, *ibid.*; H.K.Jang, *ibid.*.

- [4] M.Gronau and D.Wyler, *Phys. Lett. B* **265**, 172 (1991), I.Dunietz, *Phys. Lett. B* **270**, 75 (1991), D.Atwood, I.Dunietz and A.Soni, *Phys. Rev. Lett.* **78**, 3257 (1997).
- [5] CLEO Collaboration, M.Athanas *et al.*, *Phys. Rev. Lett.* **80**, 5493 (1998).
- [6] See for example: A.J. Buras and R. Fleischer, *Eur. Phys. J.* **C16**, 97 (2000); M. Neubert, *Nucl. Phys. Proc. Suppl.* 99, 113 (2001); J. Rosner, in *Lecture Notes TASI-2000*, World Scientific (2001); Y.Y. Keum, H.N. Li, A.I. Sanda, *Phys. Rev. D* **63**, 054008 (2001).
- [7] H.Albrecht *et al.*, *Phys. Lett. B* **241**, 278 (1990).
- [8] CLEO Collaboration, D. Cronin-Hennessy *et al.*, *Phys. Rev. Lett.* **85**, 515 (2000).
- [9] BABAR Collaboration, T.Champion, *Proc. XXXth Int. Conf. on High Energy Phys.*, Osaka, Japan, 2000, edited by C.S.Lim and T.Yamanaka (World Scientific, Singapore, to be published).
- [10] CLEO Collaboration, S.J.Richichi *et al.*, *Phys. Rev. Lett.* **85**, 520 (2000).
- [11] CLEO Collaboration, D.M.Asner *et al.*, *Phys. Rev. D* **53**, 1039 (1996).
- [12] A.Ali, P.Ball, L.T.Handoko and G.Hiller, *Phys. Rev. D* **61**, 074024 (2000).
- [13] CLEO Collaboration, R.Godang *et al.*, CLEO CONF 98-22 [in *Proc. XXIX Int. Conf. on High Energy Phys.*, Vancouver, Canada, 1998, edited by A.Astbury, D.Axen, and J.Robinson (World Scientific, Singapore, 1999)].
- [14] CDF Collaboration, T.Affolder *et al.*, *Phys. Rev. Lett.* **83**, 3378 (1999).
- [15] BABAR Collaboration, C.Jessop, *Proc. XXXth Int. Conf. on High Energy Phys.*, Osaka, Japan, 2000, edited by C.S.Lim and T.Yamanaka (World Scientific, Singapore, to be published).

Table 1: Summary of $B \rightarrow D^{(*)}K$ results. The extracted yields of $D^{(*)}K$ signals N_{DK} , their statistical significance Σ , and the obtained ratios of the branching fractions $R \equiv \mathcal{B}(B \rightarrow D^{(*)}K^-)/\mathcal{B}(B \rightarrow D^{(*)}\pi^-)$, are shown.

channel	N_{DK}	Σ	R
$B^- \rightarrow D^0 h^-$	138.4 ± 15.5	11.7	$0.079 \pm 0.009 \pm 0.006$
$\bar{B}^0 \rightarrow D^+ h^-$	33.7 ± 7.3	6.1	$0.068 \pm 0.015 \pm 0.007$
$B^- \rightarrow D^{*0} h^-$	32.8 ± 7.8	5.8	$0.078 \pm 0.019 \pm 0.009$
$\bar{B}^0 \rightarrow D^{*+} h^-$	36.0 ± 7.1	7.6	$0.074 \pm 0.015 \pm 0.006$

Table 2: Summary of the $B \rightarrow \pi\pi$, $K\pi$, KK results. The obtained signal yield (N_s), statistical significance (Σ), reconstruction efficiency (ϵ), charge averaged branching fraction (\mathcal{B}) and its 90% confidence level upper limit (U.L.) are shown. In the calculation of \mathcal{B} , the production rates of B^+B^- and $B^0\overline{B}^0$ pairs are assumed to be equal. In the modes with K^0 mesons, N_s and ϵ are quoted for K_S^0 , while \mathcal{B} and U.L. are for K^0 . Submode branching fractions for $K_S^0 \rightarrow \pi^+\pi^-$ and $\pi^0 \rightarrow \gamma\gamma$ are included in ϵ .

Mode	N_s	Σ	ϵ [%]	\mathcal{B} [$\times 10^{-5}$]	U.L. [$\times 10^{-5}$]
$B^0 \rightarrow \pi^+\pi^-$	$17.7^{+7.1}_{-6.4}$	3.1	28.1	$0.56^{+0.23}_{-0.20} \pm 0.04$	–
$B^+ \rightarrow \pi^+\pi^0$	$10.4^{+5.1}_{-4.3}$	2.7	12.0	$0.78^{+0.38}_{-0.32}^{+0.08}_{-0.12}$	1.34
$B^0 \rightarrow K^+\pi^-$	$60.3^{+10.6}_{-9.9}$	7.8	28.0	$1.93^{+0.34}_{-0.32}^{+0.15}_{-0.06}$	–
$B^+ \rightarrow K^+\pi^0$	$34.9^{+7.6}_{-7.0}$	7.2	19.2	$1.63^{+0.35}_{-0.33}^{+0.16}_{-0.18}$	–
$B^+ \rightarrow K^0\pi^+$	$10.3^{+4.3}_{-3.6}$	3.5	13.5	$1.37^{+0.57}_{-0.48}^{+0.19}_{-0.18}$	–
$B^0 \rightarrow K^0\pi^0$	$8.4^{+3.8}_{-3.1}$	3.9	9.4	$1.60^{+0.72}_{-0.59}^{+0.25}_{-0.27}$	–
$B^0 \rightarrow K^+K^-$	$0.2^{+3.8}_{-0.2}$	–	24.0	–	0.27
$B^+ \rightarrow K^+\overline{K}^0$	$0.0^{+0.9}_{-0.0}$	–	12.1	–	0.50

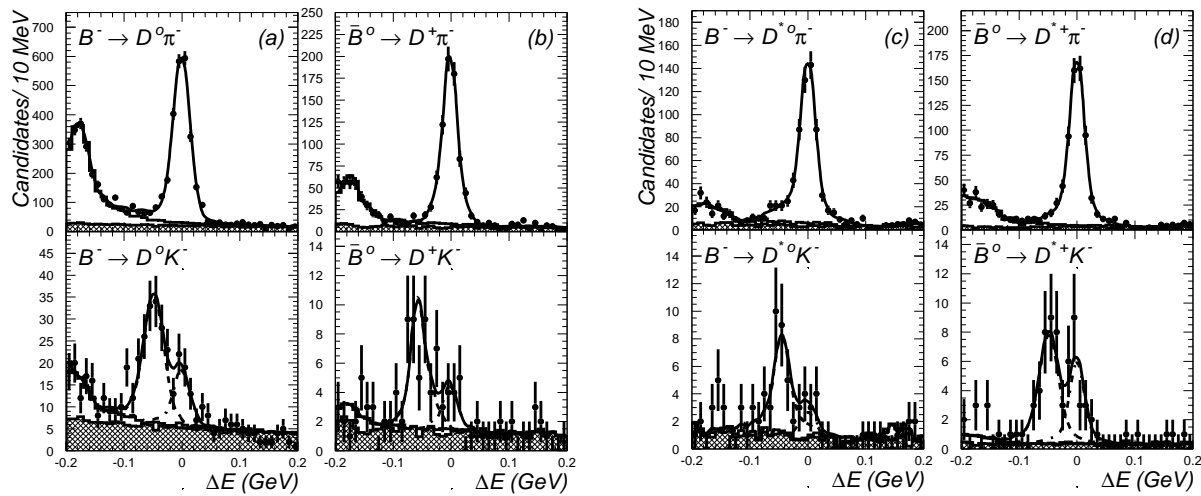


Figure 1: The ΔE distributions for the (a) $B^- \rightarrow D^0 h^-$, (b) $\bar{B}^0 \rightarrow D^+ h^-$, (c) $B^- \rightarrow D^{*0} h^-$ and (d) $\bar{B}^0 \rightarrow D^{*+} h^-$ decay channels, in the m_{bc} signal region ($5.27 \leq m_{bc} \leq 5.29 \text{ GeV}/c^2$). The top figures show $B \rightarrow D^{(*)}\pi$ control samples with the PID cut $\mathcal{R}_K < 0.8$, and the bottom figures show $B \rightarrow D^{(*)}K$ enriched samples with the PID cut $\mathcal{R}_K > 0.8$. The points with error bars present the data, the curves show the results of fits. The open histograms are the sums of background functions scaled to fit the data and the hatched histogram indicates the continuum component of the background.

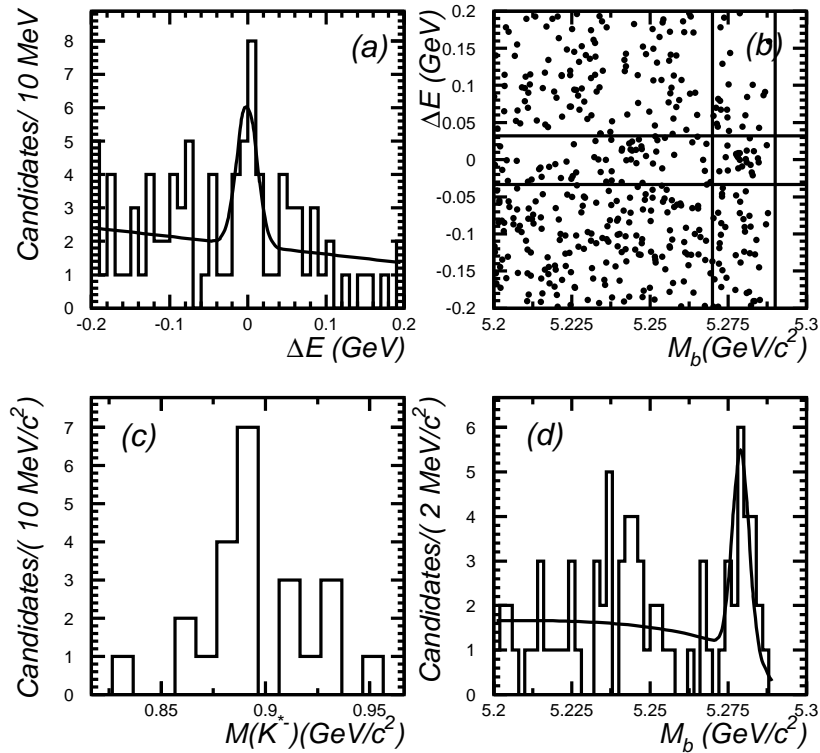


Figure 2: Plots which show evidence for the $B^- \rightarrow D^0 K^{*-}$ decay; Distributions of (a) ΔE for the m_{bc} signal region, (b) $m_{bc}-\Delta E$, (c) $K_S^0 \pi^-$ invariant mass for events in the $m_{bc}-\Delta E$ signal box and (d) m_{bc} for the ΔE signal region. The solid lines in (b) indicate the m_{bc} and ΔE signal regions.

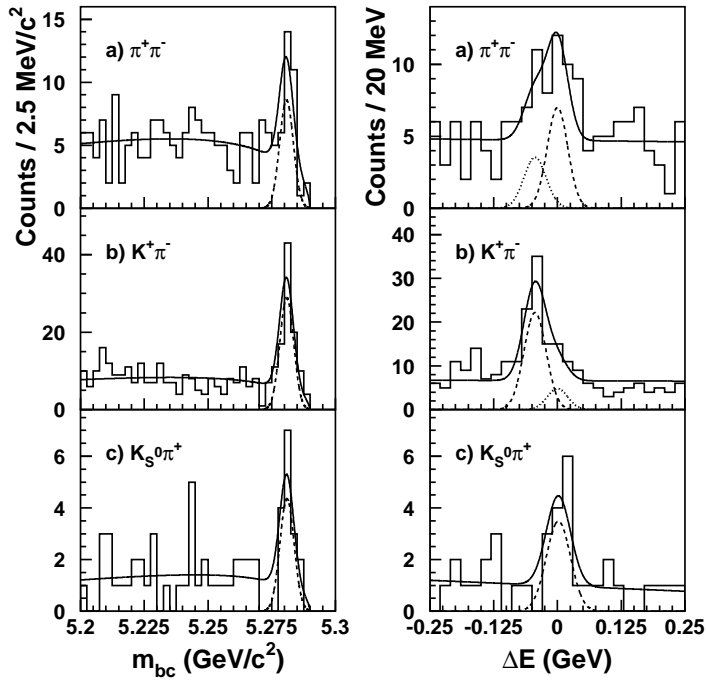


Figure 3: The m_{bc} (left) and ΔE (right) distributions, in the signal region of the other variable, for $B \rightarrow$ a) $\pi^+\pi^-$, b) $K^+\pi^-$ and c) $K_S^0\pi^+$. The fit function and its signal component are shown by the solid and dashed curves, respectively. In the $\pi^+\pi^-$ and $K^+\pi^-$ fits, the cross talk component is shown by the dotted curve.

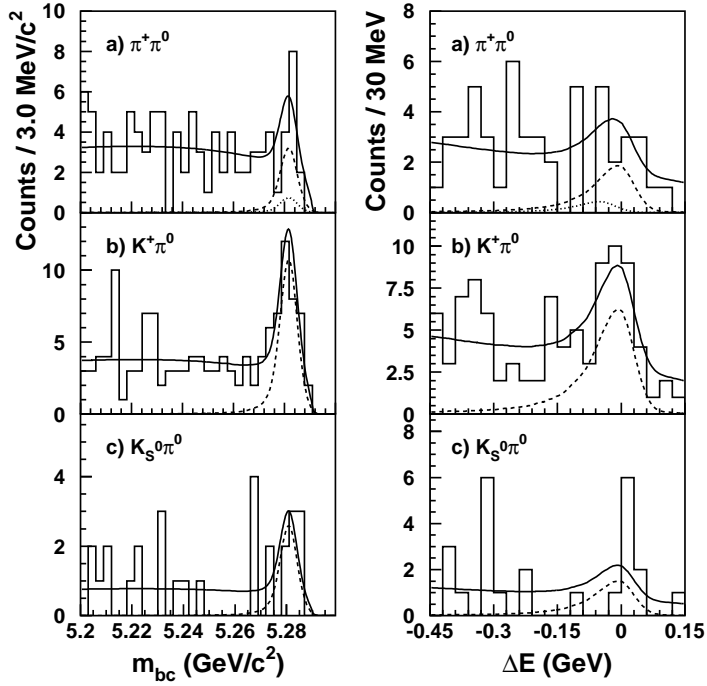


Figure 4: The m_{bc} (left) and ΔE (right) distributions for $B^+ \rightarrow$ a) $\pi^+\pi^0$, b) $K^+\pi^0$ and c) $K_S^0\pi^0$. For the $K^+\pi^0$, K mass is assumed for the charged particle. The projection of the two dimensional fit onto each variable and its signal component are shown by the solid and dashed curve, respectively. In the $\pi^+\pi^0$ fit, the cross talk from $K^+\pi^0$ is indicated by the dotted curve.

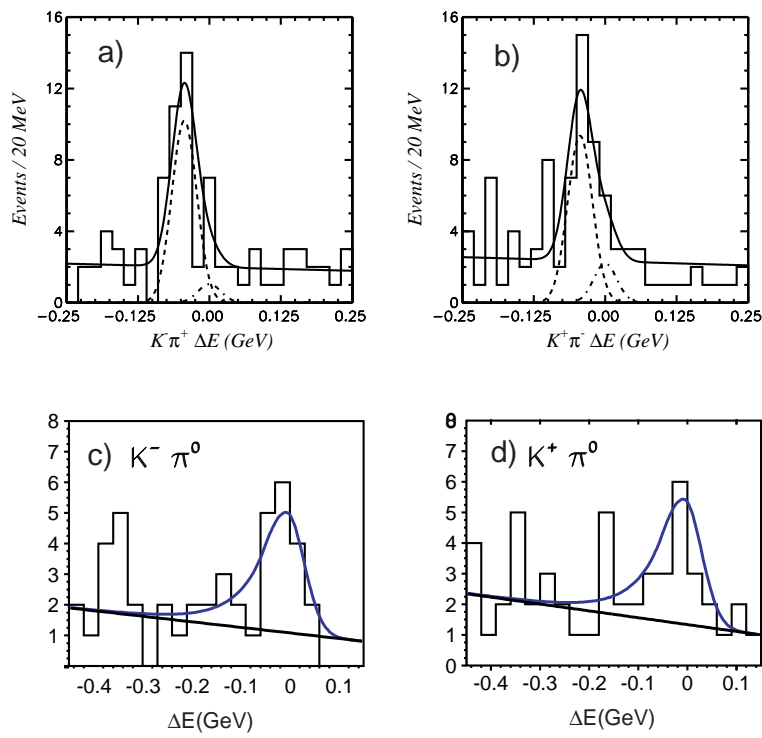


Figure 5: ΔE distribution for each a) $B^0 \rightarrow K^- \pi^+$, b) $\bar{B}^0 \rightarrow K^+ \pi^-$, c) $B^- \rightarrow K^- \pi^0$, and d) $B^+ \rightarrow K^+ \pi^0$ mode. Fits are similar to those shown in Fig. 3 and Fig. 4.

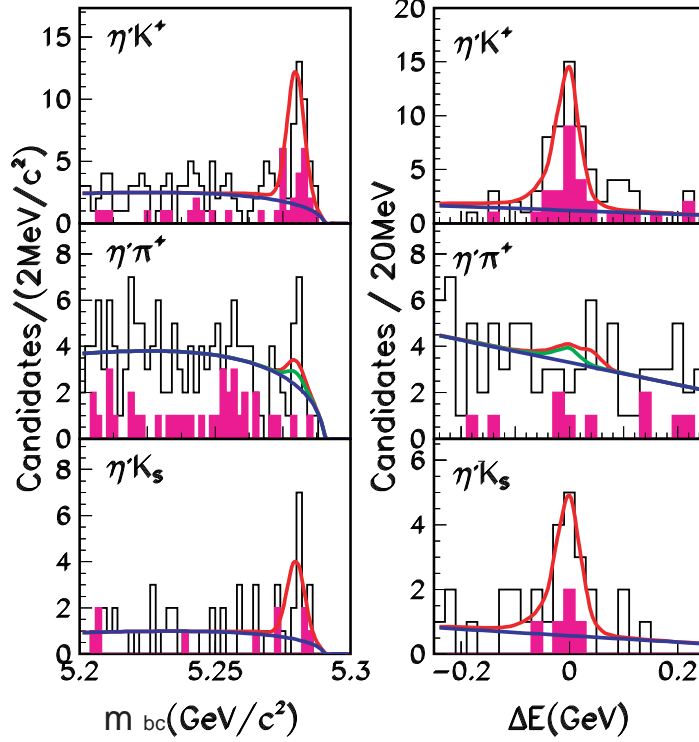


Figure 6: The m_{bc} and ΔE distributions for (top) $B^+ \rightarrow \eta' K^+$, (middle) $B^+ \rightarrow \eta' \pi^+$, and (bottom) $B^0 \rightarrow \eta' K_S^0$ mode. The hatched histograms show the contribution from $\eta' \rightarrow \rho\gamma$ sub-decay mode. The solid lines show the fits with a Gaussian signal on top of a background function, which is the ARGUS background function for m_{bc} and a linear function for ΔE . The fits for $B^+ \rightarrow \eta' \pi^+$ include the expected $B^+ \rightarrow \eta' K^+$ component.

Mode : UpperLimit

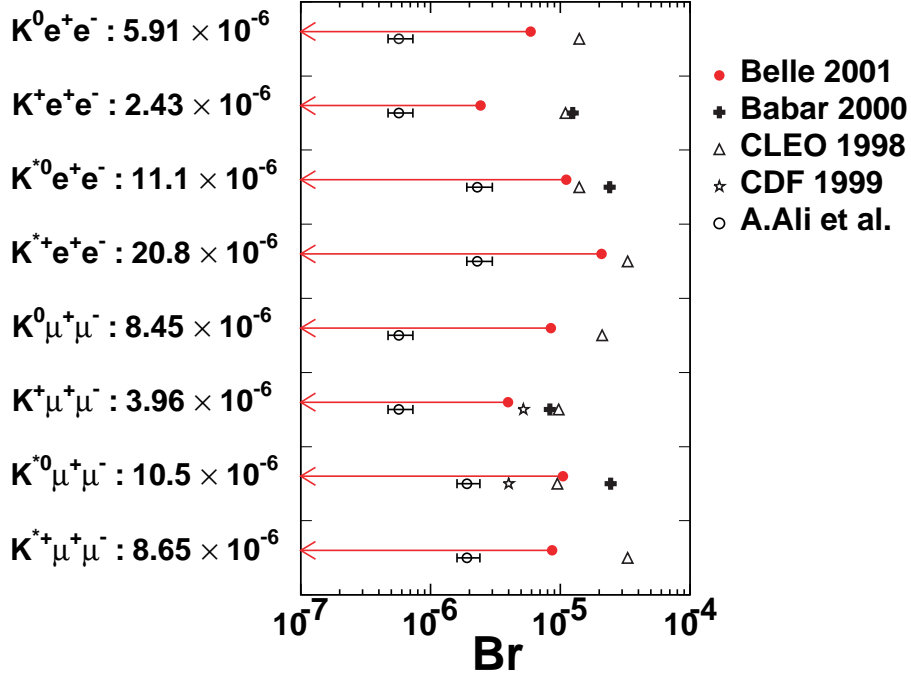


Figure 7: Upper limits on the branching fractions for each $B \rightarrow K^{(*)} \ell \ell$ mode (preliminary). Our results are compared to theoretical predictions and upper limits from previous experiments.

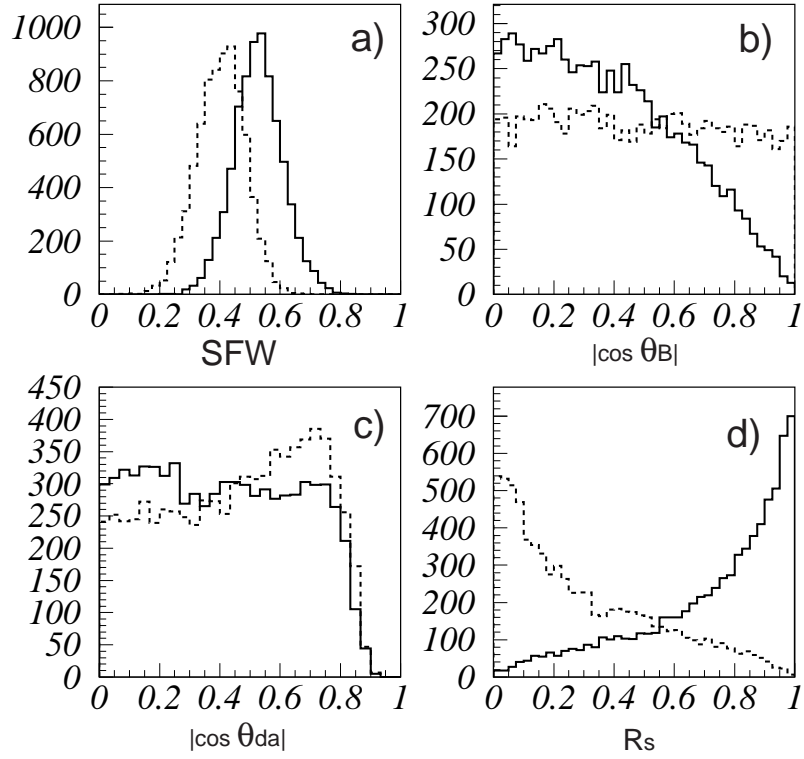


Figure 8: Distributions of the $q\bar{q}$ suppression variables in the case of $B \rightarrow \pi^+\pi^-$, $K^+\pi^-$, K^+K^- analysis; (A) SFW, (B) $|\cos \theta_B|$, (C) $|\cos \theta_{da}|$ and (D) \mathcal{R}_s . Solid and dotted lines show the distributions for the B decay signal and $q\bar{q}$ background, respectively.